

Lidar-histogram for fast road and obstacle detection

Liang Chen, Jian Yang and Hui Kong



Fig. 1. road, positive/negative obstacles and water hazards in off-road environment.

Abstract—Detection of traversable road regions, positive and negative obstacles, and water hazards is a fundamental task for autonomous driving vehicles, especially in off-road environment. This paper proposes an efficient method, called Lidar-histogram. It can be used to integrate the detection of traversable road regions, obstacles and water hazards into one single framework. The weak assumption of the Lidar-histogram is that a decent-sized area in front of the vehicle is flat.

The Lidar-histogram is derived from an efficient organized map of Lidar point cloud, called Lidar-imagery, to index, describe and store Lidar data. The organized point-cloud map can be easily obtained by indexing the original unordered 3D point cloud to a Lidar-specific 2D coordinate system. In the Lidar-histogram representation, the 3D traversable road plane in front of vehicle can be projected as a straight line segment, and the positive and negative obstacles are projected above and below the line segment, respectively. In this way, the problem of detecting traversable road and obstacles is converted into a simple linear classification task in 2D space. Experiments have been conducted in different kinds of off-road and urban scenes, and we have obtained very promising results.

I. INTRODUCTION

One of the key tasks autonomous driving vehicles have to perform is the reliable perception of their environment, such as the detection of traversable road area, obstacles and water hazards et al. In well-structured urban scenes, where the ground tends to be flat and obstacles are mostly vertical, a lot of monocular-camera or stereo-vision based approaches have been proposed to handle it. In more challenging unstructured off-road environments, 3D range data is necessary, as provided, e.g., by stereo-cameras, radars or Lidars. Recently, fully 3D Lidar scanners have been widely used in unmanned ground vehicles. Instead of sensing in a 2D plane, 3D volumes around vehicle are scanned to obtain an unordered cloud of 3D points. Lidar scanners have proven effective in off-road environment because they are able to accurately measure distance, which makes it possible to detect all kinds of obstacles and traversable area.

However, one major shortcoming in applying the 3D Lidar scanner is that the point cloud contains large number of

The authors are with the School of Computer Science and Engineering, Nanjing University of Science and Technology, Nanjing city, Jiangsu, China. Email: chinandy@foxmail.com, {csjyang, konghui}@njust.edu.cn

discrete and unordered 3D points in each frame, which makes it time-consuming for searching and indexing operations among points. Thus, it is necessary to design a fast method to roughly segment the point cloud into semantically meaningful clusters, such as traversable road plane, positive and negative obstacles, etc.

Assuming that most of the traversable region should be approximately flat, we propose a fast segmentation method to detect travaserble road area and obstacles, called the Lidar-histogram. First, we generate a Lidar-specific 2D coordinate frame in order to convert the unordered point cloud to the organized one, whch is called Lidar-imagery. The Lidar-imagery can be obtained by indexing the original unordered one to the coordinate frame. Thereafter, the Lidar-histogram can be calculated along horizontal direction in the Lidar-imagery. Fig.2 shows the Lidar-imagery and Lidar-histogram. In the Lidar-histogram, the 3D road plane in front of the vehicle is projected as a straight line segment, and the positive/negative obstacle is projected as pixels above/below the line segment. To summarize, with the Lidar-imagery and Lidar-histogram, the road, positive and negative obstacle detection problems in unordered Lidar data are converted to a simple linear classification task in 2D space. In addition, water harzards can also be deteced as negative obstacles with the help of reflectance map of Lidar sensor. By combing with a color camera, we are also able to improve road detection accuracy.

The remainder of this paper is organized as follows. Section 2 reviews some related works. Section 3 gives the derivation of Lidar-histogram and describes how it can be used for point cloud segmentation of road scenes. In section 4, the Lidar-histogram guided environment perception framework is introduced, where Lidar and camera are fused to speed up and refine the road detection performance. Experiments are conducted to verify the effectiveness of the proposed method in section 5. Section 6 concludes the paper.

II. RELATED WORKS

Papadakis[1] presented a survey of grid map based road and obstacle detection methods for unmanned ground vehicles. It states that the predominant approaches to tackle the detection problem are based on occupancy grid maps. Specifically, they rely on the analysis of 2D elevation maps, where 3D information is represented in 2D bird-view maps. Papadakis identified this as the preferred choice when dense 3D point clouds are available[2], [3]. Each cell of the grid map is associated with at least one feature vector that is computed from the 3D points. These methods to classify road area typically work well for many environments, but

are limited in general because they usually do not explicitly distinguish obstacles of different types, like rocks or grass. Another type of road and positive obstacle detection methods is based on the fusion of Lidar and image data. Shinzato et al.[4] proposed to project the Lidar points onto the image plane and then triangulate the projected points to get a graph. The local spatial relationship between points is analyzed to get the obstacles and the road is estimated by multiple free space detection. However, this method only fused the sensor information in a brute-force way because it only used the cross calibration parameter to get the Lidar points projected into the image plane. In contrast, the sensor fusion approach used in [5] is more natural. The Lidar points are firstly used to estimate the road plane with RANSAC. Then the road points are projected into the image and the corresponding image pixels are used as seeds for learning a Gaussian model. Xiao et al. [6] followed their work and fused the cues of Lidar and image in the framework of conditional random field. These methods are different from ours in two aspects: first, [4], [5], [6] project the Lidar data into the image plane using a projection matrix. However, we just need an indexing operation. Therefore, our method is much more efficient in storing for subsequent processing. Second, the points in our Lidar-imagery plane can be easily classified into three classes (road, positive and negative obstacle) via Lidar-histogram. There is no need to construct a graph model[4], estimate the plane by RANSAC[5] or train a point cloud classifier[6].

Another challenge is the negative obstacle, e.g., holes in the ground. Most works focused on the detection of positive obstacles because negative obstacles are not common in structured road environment. In general, negative obstacle is difficult to detect due to its negative nature. Lidar is thought as an effective sensor for both positive and negative obstacle detection. Heckman[7] presented a missing data interpretation based approach, in which 3D data are acquired by a Lidar. This approach includes three steps: 3D data accumulation and low level classification, 3D occlusion propagation, and context-based occlusion labeling. Larson et al. [8] also introduced a negative obstacle detection approach based on 3D Lidar. In their approach, the terrain is first analyzed and estimated, then the SVM classifier is applied to identify negative obstacles from the terrain. Shang et al. [9] presented a novel 3D Lidar setup to improve the density of scan lines and make it easier to detect the negative obstacle. In our framework , we regard the points below the road plane as the negative obstacle and we can retrieve this cue about negative obstacle from the Lidar-histogram easily.

Detection of water hazards is an important topic on obstacle avoidance for autonomous driving. Water hazards exist commonly in the off-road environment. Robust water-hazard detection methods in daytime mainly use color camera and Lidar [10], [11], where they cluster and extract water area based on color, brightness and texture features. These methods are rather complex, time consuming and cannot achieve real-time performance. Rankin et al. [12], [13], [14] and Matthies et al. [15] extract water area in wild-open areas based on the fusion of color change of water and

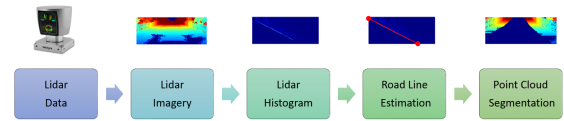


Fig. 2. The pipeline and illustration of Lidar-histogram process

the reflection of the sky. But these methods are affected by water bubble and water reflection. Shao et al. [16] applied the line structured light to detect water hazards. But the line structured light is not robust to noise or other objects which have the same reflection properties as water. In contrast, our Lidar-histogram can provide guidance for water hazards detection with the help of Lidar reflectance map.

III. LIDAR-HISTOGRAM

This section includes the procedure of extracting Lidar-histogram (Lidar-imagery, Lidar-histogram and road profile line detection) and its application (point cloud segmentation).

A. Lidar-imagery

The Velodyne HDL-64 S2 Lidar is the core 3D Lidar sensor of the autonomous driving vehicles. The sensor has 64 lasers mounted on upper and lower laser blocks, each housing 32 lasers. Both laser blocks rotate as a single unit. With this design each of the lasers fires tens of thousands of times per second, providing exponentially more data points per second and a more data-intensive point cloud than a rotating mirror design. The sensor delivers a 360° horizontal Field of View (HFOV) and a 26.8° vertical FOV. The raw output data of the Lidar are actually based on spherical coordinate system, mainly including rotation angle θ , measurement distance d , and signal strength I . The pitch angle ϕ of each laser can be loaded from the calibration file. When we convert the (d, θ, ϕ) in spherical coordinate system to the (x, y, z) in Cartesian coordinates, we can obtain a large number of unorganized points of the scene. Instead of projecting the 3D points into the 2D grid map[1], [2], [3] or the color image plane[4], [5], [6], we define a 2D coordinate system called Lidar-imagery as (θ, ϕ) , where the ϕ refers to the pitch angle, and the θ is the rotation angle. The discrete version can be written as (p, q) . This coordinate system is an image-like plane (organized map) and the “gray-level” of the “pixel” $d(p, q)$ represents the distance of the point. We can convert a point in Lidar-imagery to a 3D point according to

$$\begin{aligned} x &= d \cos \phi \cos \theta = d(p, q) * \cos(q * \delta_q) \cos(p * \delta_p) \\ y &= d \cos \phi \sin \theta = d(p, q) * \cos(q * \delta_q) \sin(p * \delta_p) \\ z &= d \sin \phi = d(p, q) * \sin(q * \delta_q) \end{aligned}$$

where δ_p and δ_q are the rotation and pitch angular resolution, respectively. Figure. 3 shows the rotation angle θ and the pitch angle ϕ in Lidar coordinate system and some Lidar-imagery results under different HFOV. The Lidar-imagery provides image-like coordinate frame to organize discrete points and it also keeps the spatial relationship between

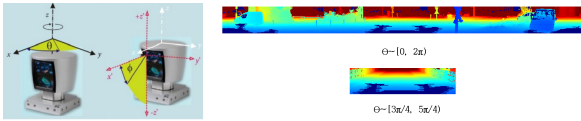


Fig. 3. The rotation angle θ and the pitch angle ϕ in Lidar coordinate frame and illustration of two Lidar-imagery results under different HFOV

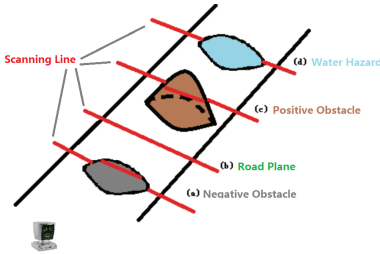


Fig. 4. The effects of different types of obstacles and road plane on the scanning line

points. It acts as an effective and efficient representation to index, describe and store Lidar data.

B. Lidar-histogram

In fact, each row in Lidar-imagery represents a Lidar scanning line. As shown in Fig. 4, different types of obstacles or road plane have different effects on the scanning line. When scanning a road plane, the measured distances from the Lidar to any points on the scanning line nearly have same value. But when it scans a positive obstacle, the measured distances of points on the positive obstacle are shorter than those on the road plane. On the contrary, the distance from the Lidar to the points on negative obstacle is longer. When scanning line meets water hazards, the emitted laser pulse usually does not bounce back to the receiver because of specular reflection, refraction, and absorption between laser and water, which usually lead to a dark region in the Lidar-imagery. Through the above analysis, the key problem is how to find the reference distance corresponding to the road plane. Inspired by the works related to the u-v disparity [17], [18],

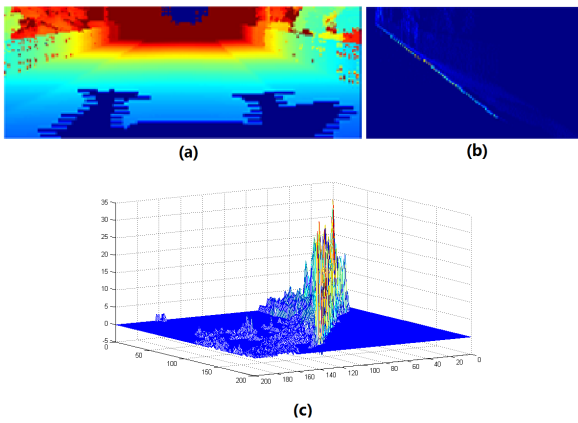


Fig. 5. (a)Lidar-imagery, (b) Lidar-histogram, (c) A 3D mesh of the Lidar-histogram.

we propose a Lidar-imagery based disparity method to find the road plane by converting the distance values (represented by the pixel values in the Lidar-imagery) to disparity values based on the following equation:

$$\Delta(p,q) = \frac{1}{x} = \frac{1}{d(p,q) \cos(q\delta_q) \cos(p\delta_p)}$$

where $\Delta(p,q)$ is the disparity of point $d(p,q)$. The u-v disparity method[17], [18] described that the 3D road plane is projected as a piecewise linear curve in the v-disparity map. As a reciprocal, we calculate the histogram based on the scanning lines in the disparity domain of the Lidar-imagery. This histogram is a row based matrix which stores the disparity values for every scanning line q .

$$v_{H,q} = \sum_{p=0}^{cols} \delta_{pq}, \delta_{pq} = \begin{cases} 1, & \Delta(p,q) = H \\ 0, & \text{else} \end{cases}$$

where $v_{H,q}$ represents the value from the histogram which accumulates the number of pixels with disparity H from scanning line q in the disparity domain. The obtained map is called Lidar-histogram although it is a 2D structure. Fig. 5(a) and (b) show a Lidar-imagery and its Lidar-histogram, we can see a straight line clearly in the Lidar-histogram, which corresponds to a dominant road plane.

C. Road Line Estimation

The weak assumption of our method is that a decent part of the area in front of the vehicle is flat. This assumption is reasonable when the measured distance is less than 30 meters in most urban and off-road environment. Actually, many other road detection methods also share the similar hypotheses. Fig. 5 (c) shows that the main part of the points lying on the line corresponds to the road plane in every scanning line. Accordingly, the road profile line can be fitted by RANSAC (Random Sample Consensus)[19] algorithm.

D. Point cloud segmentation

Thanks to the robustness of the RANSAC algorithm, we can obtain a linear model of the road plane. Without loss of generality, we assume that the equation of linear model is $y = kx + b$, where x, y are coordinates in the Lidar-histogram. Theoretically, this model can classify the point clouds into road plane, positive and negative obstacles. But in reality, road is not a perfect plane in 3D space. Taking measurement errors and the nature of nonflatness of road into consideration, we should specify a tolerance margin to contain the road points, written as

$$\begin{aligned} y &= kx + \alpha b, \quad \alpha < 1, \text{ top margin} \\ y &= kx + \beta b, \quad \beta > 1, \text{ bottom margin} \end{aligned}$$

Thus, we can obtain the classification rule for road and obstacles just as showed in Fig. 6. For the scanning line v , the bottom and top margin of its disparity can be written as $B(v)$, $T(v)$. Assuming that $D(v)$ is the disparity of a point, If $D(v) < B(v)$, this point is lower than the road plane, belonging to negative obstacle.

If $D(v) > T(v)$, this point is higher than the road plane,

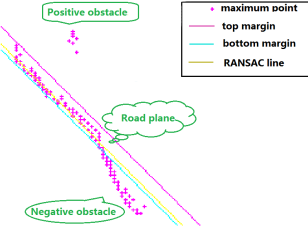


Fig. 6. Illustration of the classification rule for road plane, positive and negative obstacles.

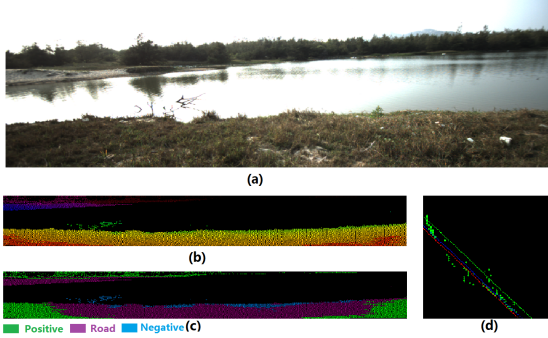


Fig. 7. The guidance information for water hazards detection.(a) is the color image of the off-road scene. (b) is the Lidar-imagery result with a big dark region.(c) is the segmentation result from the Lidar-histogram. (d) is the Lidar-histogram and the ransac result for road.

belonging to positive obstacle.

If $B(v) \leq D(v) \leq T(v)$, this point is nearly on the the road plane, belonging to the road.

Although the Lidar-histogram can not detect water hazards directly, it can provide strong cue. There exist specular reflection, refraction, and absorption when laser is projected onto water. It means that when emitted laser pulse meets water, it usually does not turn back to the receiver, which leads to a dark region in the Lidar imagery. In addition, water should lie on or below the road plane. According to these priors, there is a large possibility that a water hazard exists if there is a dark region in the area of negative obstacle or road plane in the Lidar-imagery, as showed in Fig. 7.

IV. LIDAR-HISTOGRAM BASED ENVIRONMENT PERCEPTION FRAMEWORK

Just as described above, the Lidar-histogram can play an important role in perception. However, Lidar data contains geometric information mostly, it lacks rich photometric information compared to cameras. We can not solve the perception task completely if we only rely on Lidar data. The Lidar-histogram method is simple but effective, and color image data is rich in photometric information and can be supplementary to the Lidar data. In this sense, the Lidar-histogram provides a base for combining multimodal data, where we can get seed and geometric prior from the Lidar-histogram method to help on detecting objects and segmenting regions of interest in 2D images, just like what Fig. 8 indicates. The 3D guidance information can speed up and refine the detection (segmentation) performance in color

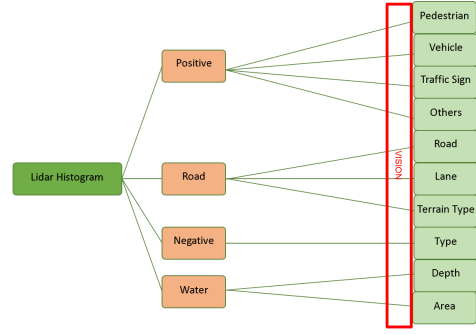


Fig. 8. The proposed framework for environment perception.

images, with the help of existing methods in data fusion, for example, graph-based models[4] or CRF-based models[6]. We take road segmentation problem as an example. First, the Lidar data can be classified into 4 classes based on our Lidar-histogram. Then, we project the road points to the color image. When processing on the color image, we only focus on the lidar-guided road region. This can reduce computational time. In addition, the geometrical feature from 3D points can help improving the performance of road segmentation.

V. EXPERIMENTS

To evaluate the performance of the proposed framework, the off-road data collected by our autonomous driving vehicle and the public KITTI-ROAD dataset[20] are used. All the experiments below are tested on a laptop platform(2*2.5 GHz, 4G RAM) and the algorithms are implemented in C/C++.

A. Road, obstacle, and water hazards detection in off-road environment

To our best knowledge, few public off-road datasets have been published. Thus we carry out the experiments on the data we collected in field tests. Our dataset contains Lidar data and color images. We use the Lidar-histogram to segment point clouds into 4 classes and corresponding color images are only used to help us to understand the scene. The Lidar imagery coordinates (θ, ϕ) in our experiments are set to

$$\theta \in [135^\circ, 225^\circ]$$

(Looking forward to keep the same view with the camera). The other parameters are $\delta_p = 0.1^\circ$, $\delta_q = 0.4^\circ$ and $\alpha = 0.5, \beta = 1.2$. The number of bins in the Lidar-histogram is 200. Fig. 9 shows the off-road experimental results under different conditions. The time cost of the Lidar-histogram procedure is about 37ms in average. More results are showed in the demo video. Experimental results show the robustness, effectiveness and high performance of the proposed framework in detection of road, positive/negative obstacles, and water hazards at the same time.



Fig. 9. Experimental results in off-road environment. Segmentation results are showed in flat(a) and nonflat(b) road condition. (c) and (d) show the negative obstacle detection results at different distance. (e) and (f) reflect that the Lidar-histogram has promising performance in water hazard detection.

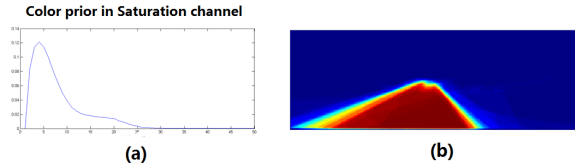


Fig. 10. Color and position distribution of road learned from the training set.

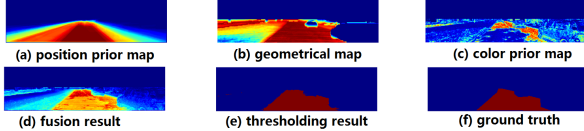


Fig. 11. Feature maps and result of the road detection algorithm.

B. Road detection in Kitti-Dataset

The KITTI-ROAD dataset includes calibration parameters, ground-truth images, and scripts for evaluation. Since most road detection approaches in literature are based on supervised machine learning techniques, the KITTI-ROAD Benchmark is divided in two datasets. The first one is the training dataset, which includes ground-truth images. The second one is the test dataset, which allows evaluation only by submission of result images to the website. These datasets comprise three different categories, namely Urban Marked (UM), Urban Multiple Marked (UMM), and Urban Unmarked (UU). Scripts provided by [20] generate a specific score for each one. These scores are the classical pixel-based metric known as Precision, Recall, False Positive Rate (FPR) and False Negative Rate (FNR), and are computed after the transformation between image domain and BEV space. As the primary metric value for comparison, the KITTI-ROAD benchmark uses F1-measure (harmonic mean of Precision and Recall) to rank all methods.

Although the approach presented in this paper does not require previous training, the performance surely will im-



Fig. 12. Visual results on road detection in KITTI-ROAD dataset.

prove if providing the training dataset to learn the optimal parameters. Because the Lidar data in KITTI-ROAD has been converted to point clouds, we can not generate the Lidar-imagery. Instead, We project the unordered point clouds to the image plane based on the cross calibration parameters. Then we calculate the Lidar-histogram in the image plane. As mentioned above, the road line is obtained with RANSAC. If the disparity of a point is close to the line, it has a high confidence that it belongs to the road. In mathematics, we can write it as $g(p,q) = 1 - |\Delta(p,q) - \Delta(q)| / |\max(\Delta()) - \min(\Delta())|$. This feature can be regarded as the geometrical prior. After calculating all pixel-level geometrical feature, we can obtain the geometrical map. Another important clue that can be calculated from the road line is the vertical coordinate of vanishing point in image. To speed up our processing, all the pixels above the vanishing point are ignored. In order to take advantage of the color images already available in the dataset. We learned the color distribution(Fig. 10(a)) in saturation channel from HSV color space and road-pixel location distribution(Fig. 10(b)) among the training dataset.

Fig. 11 shows the procedure in testing phase. We first change the color image into HSV color space and calculate the confidence for each pixel according to the learned probability density function, obtaining a color confidence map. We can also get the geometry confidence map through the Lidar-istogram and the geometrical feature. At last, we use a weighted fusion strategy to combine the three input confidence maps, and the final road detection is obtained by thresholding the fusion result with a fixed threshold value(0.5).

To show the effectiveness of the proposed Lidar-histogram algorithm, we compare the results with the Lidar based methods which can be referred ([4], [6]) in the benchmark. Fig. 12 illustrates some visual results. We can see that some areas, that are very ambiguous only based on color information, are easy to distinguish with 3D information. So with sensor fusion, we can enhance the performance. Then we evaluate the results quantitatively in the BEV space. According to the quantitative result in Table I, the performance of our method ranks first among all the methods that use lidar data and color images. This result is very promising considering that we only use very simple color feature and proposed geometrical feature. It can be regarded as the baseline for the Lidar-histogram based method. In addition, our method is very fast. It can run in realtime with a single CPU only, and easily parallelized with GPU. The specific time cost is shown in Table I.

TABLE I
RESULTS OF ONLINE EVALUATION ON KITTI-ROAD DATASET.

Category	Method	MaxF	AP	PRE	REC	FPR	FNR	Runtime	Environment
UM_ROAD	RES3D-Velo[4]	83.81 %	73.95 %	78.56 %	89.80 %	11.16 %	10.20 %	360 ms	1 core @ 2.5 Ghz (C/C++)
UM_ROAD	GRES3D+VELO	85.43 %	83.04 %	82.69 %	88.37 %	8.43 %	11.63 %	60 ms	4 cores @ 2.8 Ghz (C/C++)
UM_ROAD	FusedCRF[6]	89.55 %	80.00 %	84.87 %	94.78 %	7.70 %	5.22 %	2000 ms	1 core @ 2.5 Ghz (C/C++)
UM_ROAD	LidarHistogram(Ours)	89.87 %	83.03 %	91.28 %	88.49 %	3.85 %	11.51 %	100 ms	1 core @ 2.5 Ghz (C/C++)
UMM_ROAD	RES3D-Velo[4]	90.60 %	85.38 %	85.96 %	95.78 %	17.20 %	4.22 %	360 ms	1 core @ 2.5 Ghz (C/C++)
UMM_ROAD	GRES3D+VELO	88.19 %	88.65 %	83.98 %	92.85 %	19.48 %	7.15 %	60 ms	4 cores @ 2.8 Ghz (C/C++)
UMM_ROAD	FusedCRF[6]	89.51 %	83.53 %	86.64 %	92.58 %	15.69 %	7.42 %	2000 ms	1 core @ 2.5 Ghz (C/C++)
UMM_ROAD	LidarHistogram(Ours)	93.32 %	93.19 %	95.39 %	91.34 %	4.85 %	8.66 %	100 ms	1 core @ 2.5 Ghz (C/C++)
UU_ROAD	RES3D-Velo[4]	83.63 %	72.58 %	77.38 %	90.97 %	8.67 %	9.03 %	360 ms	1 core @ 2.5 Ghz (C/C++)
UU_ROAD	GRES3D+VELO	84.14 %	80.20 %	80.57 %	88.03 %	6.92 %	11.97 %	60 ms	4 cores @ 2.8 Ghz (C/C++)
UU_ROAD	FusedCRF[6]	84.49 %	72.35 %	77.13 %	93.40 %	9.02 %	6.60 %	2000 ms	1 core @ 2.5 Ghz (C/C++)
UU_ROAD	LidarHistogram(Ours)	86.55 %	81.13 %	90.71 %	82.75 %	2.76 %	17.25 %	100 ms	1 core @ 2.5 Ghz (C/C++)
URBAN_ROAD	RES3D-Velo[4]	86.58 %	78.34 %	82.63 %	90.92 %	10.53 %	9.08 %	360 ms	1 core @ 2.5 Ghz (C/C++)
URBAN_ROAD	GRES3D+VELO	86.07 %	84.34 %	82.16 %	90.38 %	10.81 %	9.62 %	60 ms	4 cores @ 2.8 Ghz (C/C++)
URBAN_ROAD	FusedCRF[6]	88.25 %	79.24 %	83.62 %	93.44 %	10.08 %	6.56 %	2000 ms	1 core @ 2.5 Ghz (C/C++)
URBAN_ROAD	LidarHistogram(Ours)	90.67 %	84.79 %	93.06 %	88.41 %	3.63 %	11.59 %	100 ms	1 core @ 2.5 Ghz (C/C++)

VI. CONCLUSIONS

In this paper, a fast Lidar-based road and obstacle detection method, called the Lidar-histogram, has been proposed. It can also be used to detect negative obstacles and water hazards. The pipeline of the method has five steps: the Lidar-imagery, the Lidar-histogram, road-profile line estimation, point-cloud segmentation and Bi-modal data fusion. Experiments have been conducted under different kinds of road conditions. Experimental results show that the proposed framework can achieve a realtime and promising performance.

ACKNOWLEDGMENT

The authors would like to thank the editor and the anonymous reviewers for their critical and constructive comments and suggestions. Liang Chen and Jian Yang are supported by the National Science Fund of China under Grant Nos. 91420201, 61472187, 61233011 and 61373063, the 973 Program No.2014CB349303, and Program for Changjiang Scholars and Innovative Research Team in University. Hui Kong is supported by the Jiangsu Province Nature Science Foundation (Grant No. BK20151491), and the National Nature Science Foundation of China (Grant No. 61672287).

REFERENCES

- [1] P. Papadakis, "Terrain traversability analysis methods for unmanned ground vehicles: A survey," *Engineering Applications of Artificial Intelligence*, vol. 26, no. 4, pp. 1373–1385, 2013.
- [2] A. Howard, M. Turmon, L. Matthies, B. Tang, A. Angelova, and E. Mjolsness, "Towards learned traversability for robot navigation: From underfoot to the far field," *Journal of Field Robotics*, vol. 23, no. 11-12, p. 10051017, 2006.
- [3] S. Kuthirummal, A. Das, and S. Samarakkera, "A graph traversal based algorithm for obstacle detection using lidar or stereo," in *Intelligent Robots and Systems (IROS), 2011 IEEE/RSJ International Conference on*, Sept 2011, pp. 3874–3880.
- [4] P. Y. Shintzato, D. F. Wolf, and C. Stiller, "Road terrain detection: Avoiding common obstacle detection assumptions using sensor fusion," in *Intelligent Vehicles Symposium Proceedings, 2014 IEEE*, 2014, pp. 687 – 692.
- [5] X. Hu, F. S. A. Rodriguez, and A. Gepperth, "A multi-modal system for road detection and segmentation," in *Intelligent Vehicles Symposium Proceedings, 2014 IEEE*, 2014, pp. 1365–1370.
- [6] L. Xiao, B. Dai, D. Liu, and T. Hu, "Crf based road detection with multi-sensor fusion," in *Intelligent Vehicles Symposium (IV), 2015 IEEE*, 2015.
- [7] N. Heckman, J. F. Lalonde, N. Vandapel, and M. Hebert, "Potential negative obstacle detection by occlusion labeling," in *Intelligent Robots and Systems, 2007. IROS 2007. IEEE/RSJ International Conference on*, 2007, pp. 2168–2173.
- [8] J. Larson and M. Trivedi, "Lidar based off-road negative obstacle detection and analysis," in *Conference Record - IEEE Conference on Intelligent Transportation Systems*, 2011, pp. 192–197.
- [9] E. Shang, X. An, J. Li, and H. He, "A novel setup method of 3d lidar for negative obstacle detection in field environment," in *Intelligent Transportation Systems (ITSC), 2014 IEEE 17th International Conference on*. IEEE, 2014, pp. 1436–1441.
- [10] H. Shao, Z. Zhang, K. Li, Z. Shi, D. Zhang, J. Wang, X. U. Tao, and Y. Wei, "A survey on water hazard detection in the wild field," *Computer Measurement and Control*, vol. 195, no. 44-47, pp. 5926–5948, 2014.
- [11] H. Y. Shao, Z. H. Zhang, K. J. Li, J. Wang, T. Xu, S. Hou, and L. Zhang, "Water hazard detection based on 3d lidar," *Applied Mechanics and Materials*, vol. 668-669, pp. 1174–1177, 2014.
- [12] A. L. Rankin, L. H. Matthies, and A. Huertas, "Daytime water detection by fusing multiple cues for autonomous off-road navigation," in *Proc. Army Science Conference*, 2006.
- [13] A. L. Rankin, L. H. Matthies, and P. Bellutta, "Daytime water detection based on sky reflections," in *Proceedings - IEEE International Conference on Robotics and Automation*, 2011, pp. 5329–5336.
- [14] A. Rankin and L. Matthies, "Daytime water detection based on color variation," in *Intelligent Robots and Systems (IROS), 2010 IEEE/RSJ International Conference on*, 2010, pp. 215–221.
- [15] L. H. Matthies and M. McHenry, "Detecting water hazards for autonomous off-road navigation," *Proceedings of SPIE - The International Society for Optical Engineering*, pp. 231–242, 2003.
- [16] H. Shao, Z. Zhang, and K. Li, "Research on water hazard detection based on line structured light sensor for long-distance all day," in *Mechatronics and Automation (ICMA), 2015 IEEE International Conference on*, 2015.
- [17] R. Labayrade, D. Aubert, and J. P. Tarel, "Real time obstacle detection in stereovision on non flat road geometry through disparity representation," in *Intelligent Vehicle Symposium, 2002. IEEE*, 2002, pp. 646–651 vol.2.
- [18] Y. Gao, X. Ai, Y. Wang, J. Rarity, and N. Dahnoun, "U-v-disparity based obstacle detection with 3d camera and steerable filter," in *Intelligent Vehicles Symposium (IV), 2011 IEEE*, 2011, pp. 957–962.
- [19] M. Zuliani, "Ransac toolbox for matlab," [web page] <http://www.mathworks.com/matlabcentral/fileexchange/18555>, Nov. 2008.
- [20] J. Fritsch, T. Kuhnl, and A. Geiger, "A new performance measure and evaluation benchmark for road detection algorithms," in *Intelligent Transportation Systems - (ITSC), 2013 16th International IEEE Conference on*, 2013, pp. 1693 – 1700.